Available online at www.sciencedirect.com

ScienceDirect

www.elsevier.com/locate/jmbbm

Failure analysis of sandwich-type ceramic-on-ceramic hip joints: A spectroscopic investigation into the role of the polyethylene shell component

Shinya Okita[a], *Masahiro Hasegawa*[a,*], *Yasuhito Takahashi*[b], *Leonardo Puppulin*[b], *Akihiro Sudo*[a], *Giuseppe Pezzotti*[b]

[a]*Department of Orthopaedic Surgery, Mie University, Graduate School of Medicine, 2-174 Edobashi, Tsu, Mie 514-8507, Japan*
[b]*Ceramic Physics Laboratory & Research Institute for Nanoscience, Kyoto Institute of Technology, Sakyo-ku, Matsugasaki, 606-8585 Kyoto, Japan*

ARTICLE INFO

Article history:
Received 10 December 2012
Accepted 14 January 2013
Available online 8 February 2013

Keywords:
Total hip arthroplasty
Ceramic-on-ceramic
Creep
Wear
Ceramic fracture
Raman spectroscopy
Dislodgment

ABSTRACT

The mechanisms leading to systematic failure in modular acetabular components with a sandwich insertion (alumina/polyethylene/titanium) have been reconsidered in light of the newly collected Raman spectroscopic results. Raman assessments were conducted on the polyethylene shells, which belonged to a series of six failed sandwich implants with *in vivo* lifetimes ranging between 2 and 9 yr. With only one exception, all implants commonly showed dislodgment of the polyethylene shell during radiographic analyses prior to revision surgery. The polyethylene shell slipped out of the backing titanium shell, while always remaining integer to the ceramic liner. Four implants fractured at the ceramic liners, but their fractures occurred according to distinctly different patterns, which could be rationalized and classified. The insertion of the polyethylene layer, originally conceived to reduce the rigidity of the ceramic-on-ceramic bearing and to prevent impingement between the ceramic liner rim and the femoral neck, played a role in implant failure with its initial (asymmetric) thickness reduction due to creep deformation (eventually followed by cup rotation and backside wear). The results of the present spectroscopic investigation suggest that a simplistic failure classification of the sandwich-type implant as a "ceramic fracture failure" could be misleading and might represent a confounding factor in judging about the reliability of modern ceramic implants.

1. Introduction

Through the relatively long history of alumina ceramic-on-ceramic hip bearings, the cases of fracture reported with relatively high rates could systematically be associated to design failures (Tateiwa et al., 2008). French statistics from the early seventies (Hamadouche et al., 2002; Hannouche et al., 2003; Sedel, 2000) reported a 2% fracture rate for alumina-on-alumina implants due to an unreliable fixation method adopted on the cup side. In Germany, an early design with a skirted head mated with a bulky monoblock screw cup (i.e., also referred to as the Mittelmeier design) led to fracture incidences up to 0.8% (Cameron, 1991; Huo et al., 1996; Peiro, 1991) and was abandoned by the maker in 1991. More recently, in Japan, a high fracture incidence rate in alumina ceramic-on-ceramic implants has been found for a particular "sandwich" design, which included the insertion of an adaptive layer of ultra-high molecular weight polyethylene

*Corresponding author. Tel.: +81 59 231 5022; fax: +81 59 231 5211.
E-mail address: masahase@clin.medic.mie-u.ac.jp (M. Hasegawa).

1751-6161/$ - see front matter © 2013 Elsevier Ltd. All rights reserved.
http://dx.doi.org/10.1016/j.jmbbm.2013.01.022

(UHMWPE) between the ceramic liner and the metal shell (Oonishi, 1992). In the period between 1998 and 2001 (after which the maker interrupted the supply), about 5500 implants using this hip system were replaced. Since then, several authors (Amino, 2002; Ha et al., 2006; Hasegawa et al., 2003; Kitajima and Hotokebuchi, 2003; Park et al., 2006; Suzuki, 2003) reported about catastrophic fractures at the alumina-bearing surface (ABS) of the implants from the cup side for the same sandwich-type hip implant. Owing to the phenomenological aspects of the described cases, all the failures of sandwich-type implants have commonly been referred to in the published literature as "ceramic failures" (Ha et al., 2006; Hasegawa et al., 2003; Park et al., 2006; Suzuki, 2003). Suzuki et al. (2003) mainly described problems of fracture and dislocation with the ceramic liner for the same implant studied in this paper (i.e., the ABS of the sandwich implant), while Amino (2002) reported on 5500 cases of ABS cup (January 1998–July 2000) with 16 fractures by January 2002. Kitajima and Hotokebuchi (2003) also reported more than 60 fractures by January 2003 for the ABS of the sandwich implant. These studies, reporting about a large percent of failures in sandwich-type hip implants, investigated the same implant object of the present investigation. Similarly, fractures of modular ceramic acetabular components with a sandwich polyethylene insertion (from a different maker) were recently also reported by German surgeons (Kircher et al., 2009).

While fracture of the ceramic liner component certainly represents the most evident and catastrophic phenomenon observed in a sandwich-type implant retrieved after failure, there are two important details suggesting that the actual origin of the implant failure might not necessarily reside in a poor structural behavior of the ceramic cup component. Despite the improved quality of recent ceramic implants as compared to their previous generations, it is obviously impossible to completely eliminate the risk of fracture in brittle ceramic components such as hip heads and liners. However, thoroughly compiled data reviews (excluding sandwich-type implants) indeed show that the fracture rate of third-generation alumina-bearing couples occurs at extremely low levels (Kircher et al., 2009; Tateiwa et al., 2008). On the other hand, ceramic cups usually possess by far more load-bearing capacity than the mating ceramic heads, not only because cups are mainly loaded in compression but also because, unlike balls that necessarily contain taper edges, the cup morphology can be accurately designed in order to conspicuously avoid stress intensification. Accordingly, among the sporadic events of fracture reported in the literature (Krikler, 1997; Maccauro and Piconi, 2000; McLean et al., 2002; Piconi et al., 1999; Pulliam and Trousdale, 1997; Suzuki, 2003), a large majority of cases are concerned with fractured ceramic heads rather than with ceramic liners. It follows that, if the poor strength (or brittleness) of alumina ceramic would actually have been the main cause of failure in sandwich-type implants, one could hardly explain why fracture systematically occurred on the less-stressed liner side, as reported in the majority of sandwich-type failures (Hasegawa et al., 2003; Amino, 2002), instead of hitting the most stressed regions at the corners of the head taper, which is made of the same material.

The so-called sandwich cup configuration, with its ceramic liner locked into an adaptive layer of polyethylene, was originally conceived in order to reduce the rigidity of the ceramic-on-ceramic coupling and to prevent impingement between the rim of the ceramic liner and the metal neck of the femoral stem. Various surgeons, who reported about the sandwich implant failures, observed that the liner had rotated during gait by about 90° inside the metal shell and the ball head has been displaced in superolateral direction (Hasegawa et al., 2003; Yamamoto et al., 2004). The ball head eventually entered into contact with the metal shell in the superolateral area and in a number of cases the ceramic liner fractured. In one case, fracture and fragmentation of the ceramic cup were reported (Hasegawa et al., 2003), while in another report the liner was found yet unfractured despite the implant having undergone liner rotation (Yamamoto et al., 2004). In reviewing the published literature, one might intuitively feel consensus toward authors hinting that the fault of sandwich implant failure arises from brittleness of the ceramic components (Ha et al., 2006; Park et al., 2006). The squatting attitude of Asian patients was also suggested as becoming an exacerbating factor in the fracture process (Ha et al., 2006). However, a clear and final explanation of the implant failure mechanism(s) is still missing in the literature.

We revisit here several cases of sandwich-type implant failure by focusing on the specific role played by the polyethylene shell component in the overall process of implant failure. Our opinion is that the published descriptions of ceramic liner fracture in sandwich-type implants are indeed phenomenologically correct. However, we shall also attempt to provide some clear experimental proofs supporting the thesis that the structural inadequacy of the alumina components was not the principal factor originating failure in

Table 1 – Clinical details of the six cases of sandwich-type implant failure examined in this study.

Case	Gender	Follow-up	Cause	Pristine PE thickness [μm]	Side	Inclination [deg.]	Anteversion [deg.]
I	Female	4 yr 8 months	Dislodgement fracture	3000	Left	42	−5
II	Female	9 yr 3 months	Dislodgement	5000	Right	43	16
III	Female	9 yr 8 months	Dislodgement	5000	Right	50	24
IV	Female	2 yr 11 months	No-dislodgement destruction	2000	Left	59	41
V	Female	4 yr 11 months	Dislodgement fracture	2000	right	45	25
VI	Female	9 yr	Dislodgement fracture	3000	left	51	51

sandwich-type implants. On the other hand, the structural defeat associated to creep deformation on the polyethylene side of the implants played a major role, as a consequence of the flawed joint design.

2. Experimental procedures

2.1. *Patients and implants*

Six cases of sandwich-type implant failure were examined, whose clinical details are summarized in Table 1. All retrieved implants were of the sandwich-type ABS HA Shell (CH 46)/ABS Liner (28-46)/Ball Head (28N:-4)/Perfix Stem #12-M, produced by Kyocera Co., had cementless fixation, and belonged to female patients. The fact that all samples belonged to female patients, however, was just due to a fortuitous circumstance and it is believed not to limit the possibility of extending the outputs of the present investigation to eventual cases of male patients. The *in vivo* implantation lifetime of the devices ranged between 2 yr 11 months and 9 yr 8 months, for an average followup of 6 yr 9 months. No traumatic event, as possible cause of failure, was encountered in all patients. The time delay between symptoms of failure and revision typically ranged between few days and few weeks. Except for the shortest followup (Case IV in Table 1), all the studied retrievals showed dislodgment of the liner at the time of revision surgery. However, in two of the six studied retrievals (Cases II and III) the ceramic liner did not fracture. Among the four cases in which the ceramic liner fractured, Case IV was completely different from the other cases because it showed fragmentation of the ceramic liner into many small pieces. Anteversion and inclination angles for all the studied cases are listed in Table 1, as obtained from radiographic analyses immediately after primary surgery. As far as inclination angles are concerned, a range comprising between 30° and 50° is considered to be a safe zone for avoiding dislocation, while for anteversion the angular range is between 5° and 25° (Lewinnek et al., 1978; Widmer and Zurfluh, 2004). Therefore, only Case IV, for which radiographic analyses showed an inclination angle of 59° (cf. Table 1), should be considered affected by the effects of an excessive inclination. Values of anteversion angle, which could not be considered in the safe zone, included Cases I, IV and VI. In particular, the anteversion angle $\approx -5°$ of Case I clearly represented an implantation error.

2.2. *Raman spectroscopic assessments on retrievals and their preliminary calibrations*

Raman spectra were collected with a triple monochromator spectrometer (T-64000, ISA Jobin-Yvon/Horiba Group, Tokyo, Japan) equipped with a charge-coupled detector (i.e., a high-resolution CCD camera). The laser power at the UHMWPE surface was typically 90 mW. The laser excitation source was a monochromatic blue line emitted by an Ar-ion laser at a wavelength of 488 nm. Spectral integration times were typically 5 s for unpolarized spectra. Each recorded spectrum was averaged over three successive measurements at each selected location. The confocal configuration of the probe adopted throughout the present experiments corresponded to a $\times 100$ objective lens; numerical objective aperture, confocal pinhole diameter, and focal length of the objective lens were set as NA=0.9, $\Phi = 100\,\mu m$ and $f = 0.3\,mm$, respectively. All Raman spectra were non-destructively recorded at room temperature. Intensity and full-width at half-maximum (FWHM) of the 1130 cm^{-1} Raman band of polyethylene were retrieved by fitting the CCD raw data to the mixed Gaussian/Lorentzian curves with commercially available software (Labspec, Horiba Co., Kyoto, Japan). Variations of FWHM with respect to a virgin sample reflected the microstructural modifications induced by body weight, namely by the uniaxial residual strain piled up in

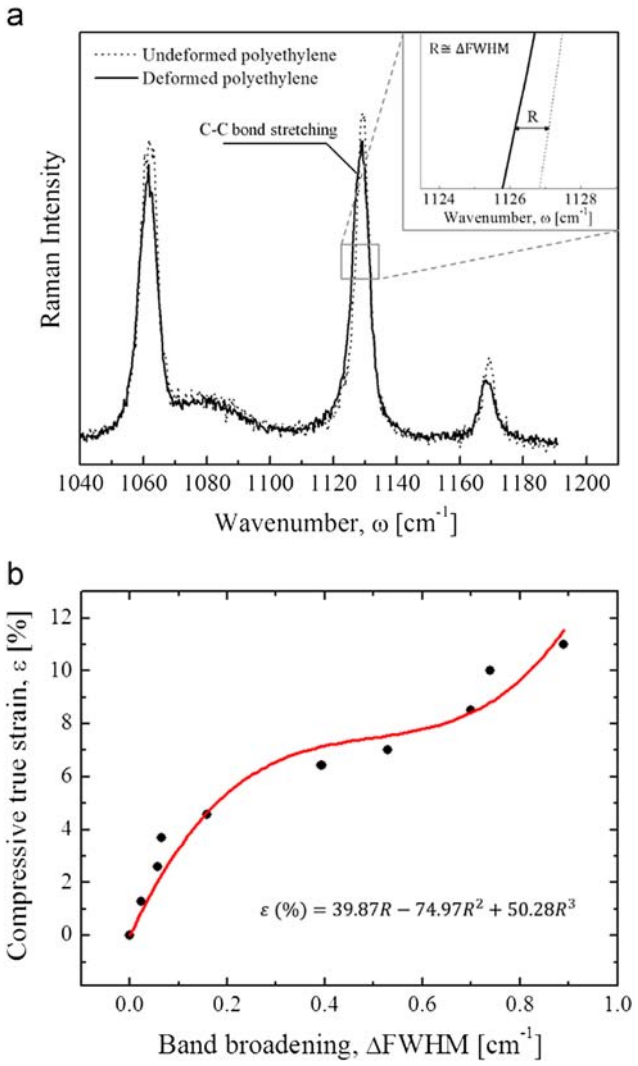

Fig. 1 – (a) Raman spectra are shown of the investigated polyethylene layer belonging to the sandwich-type implants in its unstrained and compressively strained state. In the inset, an enlargement of the spectral region is given where band broadening was measured. Note that R ≈ ΔFWHM because broadening occurred mainly from the low-frequency side of the band and (b) plot of band broadening vs. compressive true strain as obtained by preliminary calibration tests of uniaxial compression on undeformed samples. The cubic equation best-fitting the experimental plot is given in the inset.

the polymeric structure. The width of the Raman band located at 1130 cm^{-1} (A_g+B_{1g} mode or symmetric stretching of C–C bonds (Tashiro et al., 1988; Wong and Young, 1994)) was selected as a sensor for residual strain in the polymeric network because it reflects the degree of disorder of the polymeric network and its degree of molecular orientation, which are both directly affected by strain. Fig. 1(a) shows the Raman spectrum of the undeformed polyethylene of the sandwich-type implant under investigation vs. that of the same material deformed with a true strain of 11%. A clear broadening could be observed (cf. also inset) for the C–C bond-stretching band located at around 1130 cm^{-1}. Band broadening, characterized by the variation of FWHM, could be rationalized as a function of true residual strain by means of a cubic dependence, as given in the calibration plot of Fig. 1(b) (cf. best-fitting equation in inset). In the latter plot, uniaxial strain (in a known amount) was intentionally introduced into a pristine (undeformed) sample and Raman band-broadening measured after 24 h recovery since successive sample unloading. The plot, thus, reports about the dependence of broadening of the C–C stretching Raman band on the amount of the compressive (uniaxially applied) residual strain permanently stored in the material. The increase of structural disorder under compressive strain in turn reflects in a broadening of the Raman band due to both inter- and intra-lamellar slip processes in fractions depending on the amount of strain. Additional phenomena leading to broadening of the Raman bands have also been indicated, including crystallite fragmentation, fibril formation, and chain disentanglement (Hiss et al., 1999). These microstructural modifications generally appear at relatively high strain levels, while broadening of the 1130 cm^{-1} band rigorously obeys a linear dependence only at low strain levels, as shown in band-width/strain calibrations in previous papers (Kumakura et al., 2009; Kyomoto et al., 2007; Pezzotti et al., 2011). The threshold for deviation from a linear behavior, namely for the activation of multiple microscopic mechanisms of deformation, strongly depends on the polymer microstructure and, thus, varies from material to material. A comparison between the polyethylene material investigated in this paper and the newest brands of polyethylene materials with engineered microstructures more recently launched in the orthopedic market is definitely beyond the scope of this paper. However, we wish here to qualitatively mention about a comparison (not shown here) we could make based on plots similar to those shown in Fig. 1(b). The comparison demonstrated that the polyethylene material used in the sandwich-type implants was a relatively "soft" one, presumably due to its lower crystallinity and lower degree of cross-linking as compared to modern polyethylene materials. According to the complex deformation behavior followed by the material investigated in this paper, transformation of band broadening data into strain values was performed by means of the cubic calibration curve obtained in Fig. 1(b).

Exploiting the high transparency of polyethylene, non-destructive in-depth scans allowed us to retrieve detailed sub-surface profiles of spectral properties at selected locations along the entire thickness of the polyethylene shells. In the experimental practice, an automated sample stage with sub-micrometric step precision was employed, making it possible to record spectra at each depth focusing below the sample surface, and to map spectral features with lateral line scanning on the sample surface and along the sub-surface. Maps $30 \times 30\ \mu m$ were typically recorded at 50 different depths for each polar angle of the shell, and the collected spectra (900 spectra for each map) averaged to give the representative molecular vibrational modes of the polyethylene structure at each selected in-depth location. Measurements of sub-surface profile properties were eventually repeated at nine polar angles along a circumferential path in a plane containing the axis of symmetry of the cup and passing through the main-wear zone. The locations were thus separated by an angular displacement of 22.5°. Mapping rather than single-point measurements was made in an attempt to improve the statistical validity of the strain assessments at each selected location of the investigated

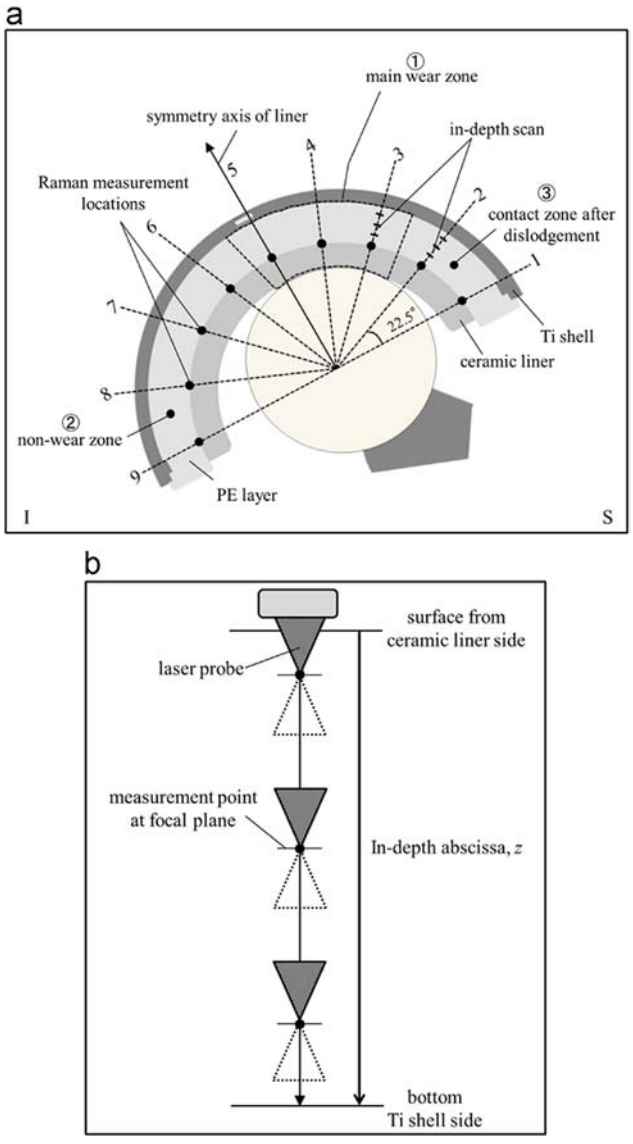

Fig. 2 – (a) Schematic draft describing the geometrical characteristics of the sandwich-type implant studied and the protocol followed in the quantitative analysis of creep displacements in its polyethylene layer and (b) explanatory draft of the in-depth defocusing experiments used for assessing the residual strain profile developed along the thickness of the UHMWPE layer at a given location as shown in (a).

retrievals. The draft in Fig. 2(a) shows the geometrical locations of the Raman measurements, while the in-depth (or defocusing) scan protocol followed at each measurement location is given in Fig. 2(b). Strain data at each polar location were translated into thickness variations due to creep by integrating the in-depth strain profile over the in-depth abscissa through the entire thickness of the polyethylene layer at each measurement location. The method is schematically explained in Fig. 2(b), and the related computational procedures were previously shown (Kumakura et al., 2009). In this study, the total number of collected Raman spectra on all retrievals was in the order of $\approx 2.5 \times 10^6$ for a total measurement time of ≈ 2100 h. Finally, it should be noted that the Raman method for assessing creep displacements in acetabular cups is relatively new (Kumakura et al., 2009; Pezzotti et al., 2011) and yet lacks a direct validation according to more conventional methods based on profilometry analyses. However, such latter analyses, considered as the golden standard method in hip arthroplasty, can only record total thickness reductions and are, thus, comprehensive of both creep displacements and wear thickness consumptions. This makes a direct comparison between profilometry and Raman results difficult, the latter ones including only creep displacement contributions. Nevertheless, an indirect confirmation of the Raman method for creep analysis was provided in a previous study (Pezzotti et al., 2011), in which some of the retrieved cups were exposed for very short periods of time in the human body and, thus, mainly underwent creep deformation. In such cases, a good correspondence could be found between Raman analyses of creep displacements and thickness reductions measured by standard methods.

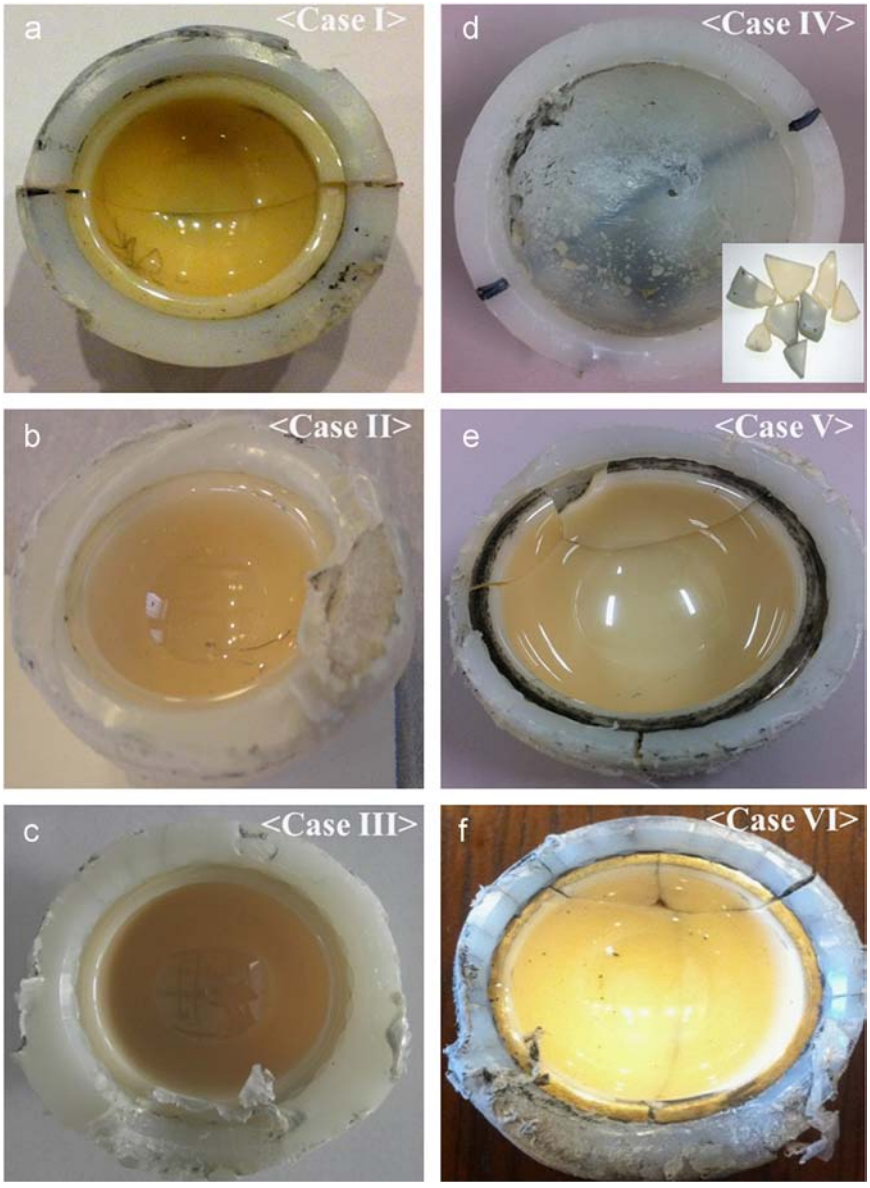

Fig. 3 – Photographs of the ceramic-cup/polyethylene-shell components of the investigated sandwich-type implants after being retrieved from the patients' body. In Case IV, destruction of the ceramic liner occurred *in vivo* (cf. photograph of the ceramic broken pieces in the inset of (d)).

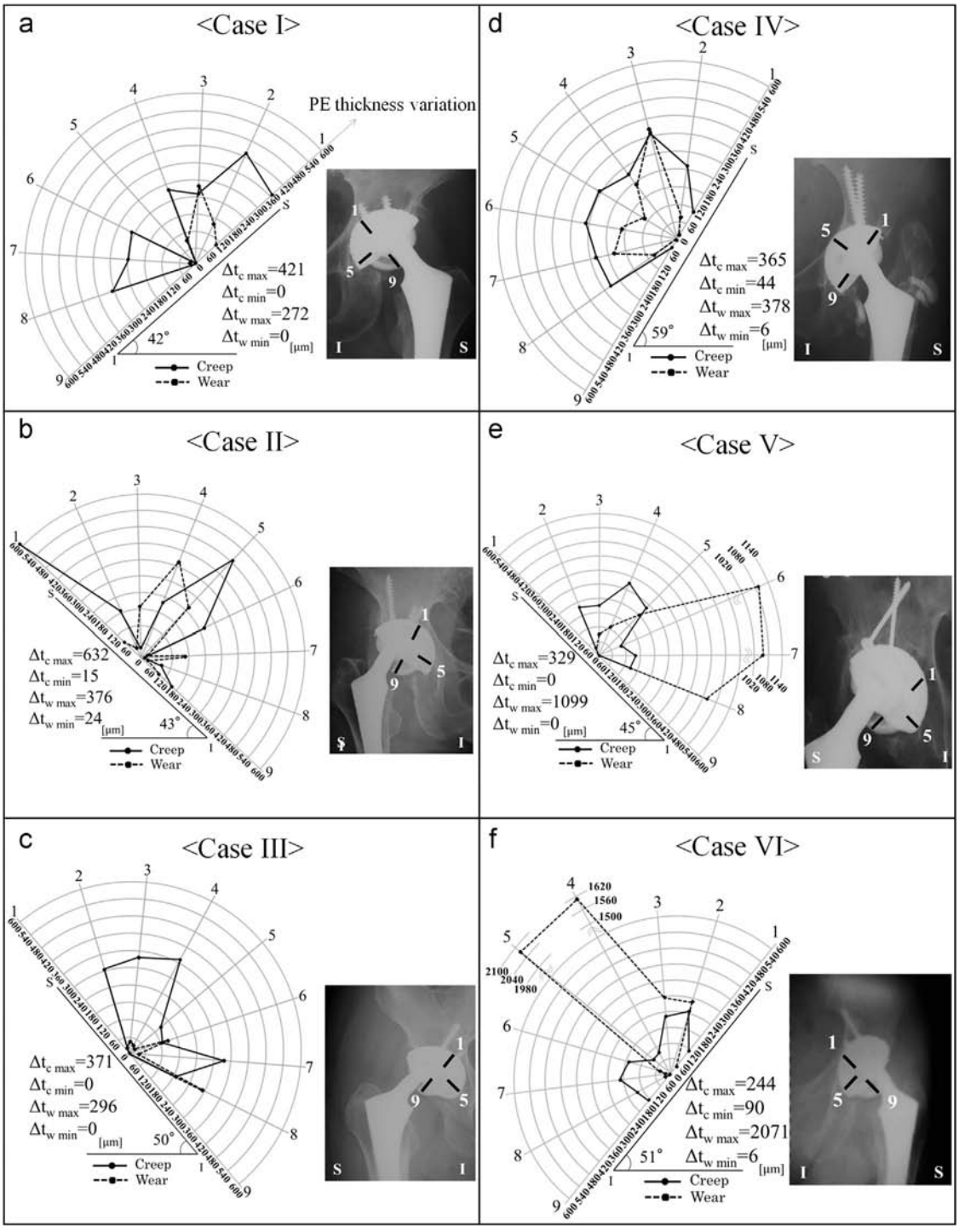

Fig. 4 – Polar plots of the total creep and wear displacements recorded along a circumferential path of the UHMWPE shell of the investigated implants. Inclination angles are also shown for better clarity. Radiographic analyses are shown as collected immediately before revision surgery. The numbers shown in inset of the radiographs correspond to the numbers locating the radial directions in each polar plot.

3. Results and discussion

3.1. *Phenomenology of the failure cases*

The photographs in Fig. 3(a)–(f) represent the ceramic-cup/polyethylene-shell components of the investigated failed implants after being retrieved from the patients' body. The results of radiographic examinations immediately before revision surgery are shown for each of the studied Cases in Fig. 4. Case I in Table 1 (Figs. 3 and 4(a)) was revised after dislodgment (namely a clearly visible shift of the joined ceramic/polyethylene parts out of the metal shell). The cause

of failure was simply classified as "dislodgment", although the retrieval also showed a clear-cut circumferential fracture trajectory dividing the ceramic liner into two distinct parts of about the same size (cf. Fig. 3(a)). The two cases labeled II and III in Table 1 were revised due to liner dislodgment (cf. Fig. 3(b) and (c), respectively, with radiographic analyses in Fig. 4(b) and (c)), and showed no fracture of the ceramic liner. Among the remaining three cases, Case IV showed no visible dislodgment (Figs. 3 and 4(d) for Case IV), but its ceramic liner fractured with extensive fragmentation (cf. photograph of the broken pieces of the ceramic liner in inset of Fig. 3(d)). The many broken ceramic pieces needed to be retrieved separately from the implant in the body of the patient. Cases V and VI both underwent dislodgment (Fig. 3(e) and (f), respectively; radiographs shown in Fig. 4(e) and (f), respectively) and fracture of the respective ceramic liners. However, important differences could be noted in comparing the fracture patterns of the latter two ceramic liners as compared to the other fractured liners. Case V showed three broken (chipped) pieces at the rim of its ceramic liner, but unlike Case I no circumferential fracture path was observed. On the other hand, the fracture pattern in Case IV was somewhat merging the patterns found in Cases I and V, with the display of both edge chipping (into two pieces) and a main circumferential fracture path. The different fracture pattern represents an important difference, which most likely differentiates the mechanisms leading to the catastrophic failure events occurred *in vivo* in different implants, and which will be discussed in forthcoming Section 3.3. In all cases of dislodgment, we never observed any (even local) detachment between the UHMWPE shell and the ceramic liner. Both components thus shifted with remaining integer to each other. Except for Cases I and IV, the polyethylene shells showed significant damages, including severe abrasive wear especially localized at the rim area, in which significant residual deformation also locally occurred, possibly due to creep. In a purely mechanistic view, the damages appeared similar to those reported earlier by Messieh et al. (1994) in describing wear debris originated from the contact of a bipolar cup with the femoral neck. Some circumferential cracks were also visible near the edge of the polyethylene shell belonging to Cases V and VI. Cases II, III, and VI showed severe delamination and flaking of the polymeric structure mainly at the contact area between the shell and stem, but also in other zones around the circumference of the shell. Kaku et al. (2001) described phenomenologically similar microfracture events and damages for the polyethylene liner of a bipolar femoral head. Moreover, our data seem to confirm a thesis put forward by Yamaguchi et al. (2000) in reviewing a large number of acetabular components. These researchers found that cups with impingement were systematically more anteverted than those without impingement. As a matter of fact, we also found significant UHMWPE damage due to impingement in Cases IV and VI, which were the implants with the highest anteversion angle in the studied series of retrievals. Besides promoting subluxation and dislocation of the femoral head, prosthetic impingement was reported to significantly contribute to implant loosening by imparting eccentric loads to the cup and by the direct production of polyethylene wear debris (Coventry, 1985; McCollum and Gray, 1990; Woo and Morrey, 1982). We shall indeed show in the following sections that local impingement might have played a detrimental role also in sandwich-type implants by promoting sliding of the UHMWPE layer (always integer to the ceramic shell) and, thus, leading to the observed common dislodgment of the polyethylene and ceramic parts. As far as the inclination angle was concerned, it is conceivable to expect a higher creep deformation in the zone near the edge of the UHMWPE liner in the implants with high inclination angle.

3.2. *Creep and wear analyses of retrieved polyethylene shells*

Following the Raman confocal procedures described in Section 2.2, spatially resolved profiles of the strain field that permanently remained stored in the UHMWPE shells of the retrieved sandwich-type implants could be measured and displayed in polar plots as a function of sample depth along the entire thickness of the shells. Note (from Table 1) that the pristine thickness of the UHMWPE shell was different for different implants, despite all implants being from the same maker. An intermediate thickness of 3 mm (Cases I and VI), a minimum thickness of 2 mm (Cases IV and V) and a maximum thickness of 5 mm (Cases II and III) were the three patterns available in the examined retrievals. In Fig. 4, polar plots are shown, for each of the examined retrieval, of the total creep displacements recorded along a typical circumferential path of the UHMWPE shell. The examined circumferential path crossed the main wear zone of the bearing surfaces. Creep displacements could be obtained by numerically integrating over the entire thickness of the shell the respective in-depth strain profiles, according to a procedure explained in previous publications (Kumakura et al., 2009; Pezzotti et al., 2011). In-depth strain profiles were in turn non-destructively retrieved from FWHM data analyses of the Raman band of UHMWPE representing symmetric stretching of the C–C bonding. In the polar plots, the inclination angle of the acetabular cup of each implant is also represented for better clarity, as given in Table 1. It was already mentioned in Section 2.2 that the numerical integration, performed for calculating local creep displacements, encompassed profiles of fifty points for each polar angle, while data points at each depth represented an average value retrieved over 900 spectra. The thickness reductions that arose from creep deformation, Δt_c, and wear abrasion, Δt_w, as they piled up during the *in vivo* lifetime are represented in Fig. 4 by full and broken lines, respectively. Numerical values of both creep displacements and worn out thicknesses as measured at different locations in each retrieval are also explicitly listed for better clarity in Table 2. The Δt_w values were obtained by subtracting the measured, Δt_c, from the pristine cup thickness at each location of the polar plot. In the previous section, it was described that no detachment between the UHMWPE shell and the ceramic liner was observed in the investigated retrievals. Therefore, different from the usual definition of abrasive wear between ceramic and polyethylene bearings, the wear damages reported in this paper unequivocally refer to the occurrence of backside wear due to friction between the Ti-metal shell and the UHMWPE shell. A proof for this

Table 2 – Numerical values of thickness reduction in six cases of UHMWPE shells as detected at different polar locations in the nominal main wear zone. Thickness reductions are differentiated into separated components due to creep and backside wear, the former ones obtained by Raman spectroscopic assessments.

	Creep displacement, Δt_c [μm]								
	Measurement point								
Case	1	2	3	4	5	6	7	8	9
I	362	421	256	275	0	250	241	316	0
II	632	185	41	223	484	249	15	80	156
III	0	304	344	371	160	124	344	180	0
IV	112	250	365	277	305	307	282	275	44
V	0	221	214	329	290	116	163	156	0
VI	118	244	214	99	90	178	187	149	120
	Worn out thickness, Δt_w [μm]								
	Measurement point								
Case	1	2	3	4	5	6	7	8	9
I	109	163	272	95	0	16	16	17	0
II	94	46	187	376	258	24	170	24	92
III	0	29	58	34	24	146	41	296	0
IV	6	79	378	233	137	189	227	103	15
V	0	29	96	121	240	1099	1052	504	0
VI	38	286	296	1614	2071	44	20	25	6

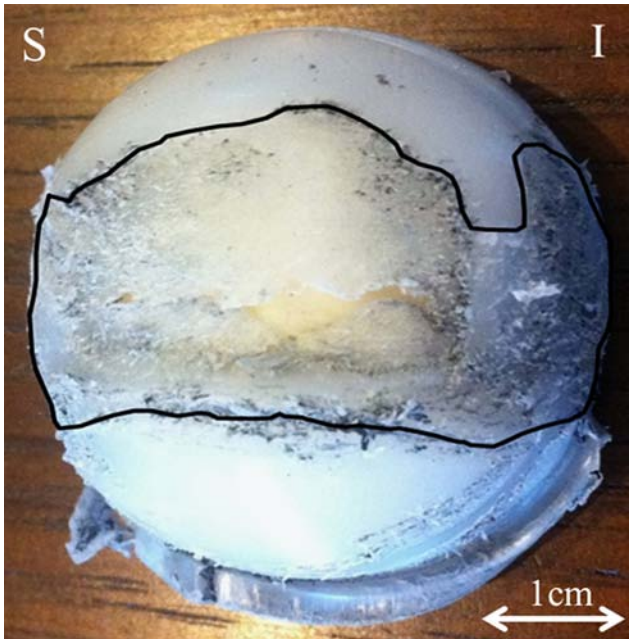

Fig. 5 – Evidence for backside wear in the polyethylene layer of Case V. The abraded area has been highlighted with a black contour for better visualization.

assertion is given in the photograph in Fig. 5. However, it is anticipated at the outset that a comprehensive interpretation of the data shown in Fig. 4 might be quite complex due to the fact that we could only access to final thickness variations, without the knowledge of the temporal sequence at which such variations occurred (i.e., in particular at which stage of dislodgment they occurred). Moreover, different implants showed quite different patterns of creep and wear damages in terms of the respective thickness reductions. Nevertheless, some important evidences could be collected, which can be summarized as follows:

(i) In comparing different retrievals, it immediately appears evident that the thickness reductions due to backside wear in Cases V and VI were exceptionally high as compared to the other retrievals examined. However, while in Case VI the maximum wear damage measured ($\Delta t_{w\ max}$=2.071 mm) occurred in correspondence of a location where one would approximately expect the occurrence of the main wear zone, in Case V the maximum wear damage ($\Delta t_{w\ max}$=1.099 mm) occurred at a location corresponding to what one would expect to be the non-wear zone of the cup at the time of implantation. Both implants indeed showed substantial dislodgment, but the difference in the observed locations of wear patterns suggest that, unlike Case VI, abrasive backside wear in the UHMWPE shells of Case V occurred after slip of the UHMWPE shell out of the Ti-alloy shell. This speculation is partly confirmed by the fact that in Case VI significant damage of the UHMWPE shell appeared in the rim area as a consequence of stem impingement during gait (after rotation of the ceramic/UHMWPE components inside the metal shell), while the shell in Case V showed no damage at its rim but it was severely abraded in its backside zone due to impingement on the edge of the metal cup after dislodgement (cf. Fig. 3).

(ii) Both Cases II and III, which by design incorporated the thickest UHMWPE component in their pristine state, showed significant abrasive damage at the rim of the UHMWPE shell (i.e., by impingement of the stem). The *in vivo* times of these two implants were nearly the same and also the longest in the studied series. Both implants showed pronounced dislodgment at the time of revision surgery, but no fracture of the ceramic cup. The occurrence of backside wear was quite limited and localized in both implants, suggesting that dislodgement occurred suddenly. However, peculiar to Case II was a quite high creep displacement at the upper edge of the UHMWPE shell, due to severe impingement by the femoral head at the onset angle for subluxation.

(iii) Case IV, which showed no dislocation and destruction of the ceramic liner, was the only implant in which creep deformation was quite homogeneous in the polar rotation interval encompassing gait motion (all other implants showed inhomogeneous distributions of creep displacements with maximum values at variable inclination angles). We shall associate the lack of localized deformation in the UHMWPE shell of Case IV to the absence of dislodgement. Despite being the implant with the shortest exposure *in vivo*, the implant of Case IV showed creep displacements comparable with those measured in the long-term retrievals analyzed. This observation confirms the notion that creep deformation in polyethylene hip components mainly occurs during the initial time (<2 yr) from primary surgery (Bewill et al., 2005; Glyn-Jones, 2008).

The results shown in Fig. 4 help visualizing a significant creep contribution to the *in vivo* penetration of ceramic liner component into the Ti-metal shell as a consequence of local flattening of the polyethylene shell. The general conclusion drawn from the examination of Δt_c data in comparison with the overall displacements, Δt, is that, at the time of explantation, the creep flattening contribution in the UHMWPE shell could be locally as large as one third of the entire UHMWPE shell thickness. Such large creep displacements were not only responsible for the linear penetration of the ceramic liner into the metal shell, but also for the successive patient weight redistribution with application of an asymmetric (incorrect) loading to the ceramic liner.

An interesting finding could be obtained by examining the residual strain profiles in Case VI, as developed along the subsurface of the UHMWPE layer of the retrievals. We examined the strain profiles developed at three characteristic zones; namely, the main wear zone, the non-wear zone, and the contact zone after dislodgement (labeled (1), (2), and (3), respectively in the draft of Fig. 2), which corresponded to the angular sectors labeled 3–4, 8–9, and 1–2 in Fig. 2(a), respectively. A low (and conspicuously constant) level of residual strain was found along the thickness, as expected, in the non-wear zone. Moreover, the magnitude of the total

thickness reduction due to residual strain was similar in the main wear zone and in the contact zone after dislodgement (both in the order of the hundreds of μm; cf. Table 2). However, such thickness reduction arose from residual strain profiles with quite different morphologies. Fig. 6 shows a comparison among the three strain profiles mentioned above. In zone (1), a maximum was found at about 700 μm in the sub-surface, while in zone (3) the strain level was constant along the sub-surface. This interesting detail is in agreement with the previous studies of residual deformation in the polyethylene liner of conventional hip implants (Pezzotti et al., 2011) and suggests that the profile of residual strain piled up during *in vivo* cycling load, namely upon regular deambulation, can be differentiated in the experimental practice from that piled up under abnormal loading conditions (i.e., local impingement after liner dislodgement).

3.3. *Failure mechanisms in sandwich-type ceramic-on-ceramic implants*

In a recent paper, Dalla Pria et al. (2010) have reviewed the topic of breakage of ceramic-on-ceramic hip couples. Although none of the reviewed implants belonged to the sandwich-type studied here, extensive discussions and classifications were given of fracture patterns in ceramic liners, which present interesting aspects and provide guidance in the context of this paper. Two main types of fracture mode were reviewed: (i) the so-called "undetected fracture" of the liner, in which circumferential fracture occurred into two parts above the conical coupling, with no fragments (Sariali et al., 2009); and, (ii) the rim fragmentation (or chipping) fracture which arises from neck impingement against the rim of the ceramic liner upon subluxation (Ha et al., 2006; Willmann, 2001). The above-referred type (i) of fracture is quite unusual and was not observed in our investigation. In type (ii), even assuming the ceramic liner being correctly positioned in the metal shell, a combination of shocks and edge loading by the ceramic head was designated as responsible for rim breakage, which is indeed what we have observed in Cases V and VI (cf. Fig. 3(e) and (f)). Chipping of the liner has been reported to occur when the inclination angle is too steep or when the anteversion angle is out of the safe zone (Hasegawa et al., 2006; Widmer and Zurfluh, 2004; Willmann, 2001). This was obviously the case in retrieval Case VI, which showed both inclination and anteversion angles at the limit of the safe zone. On the other hand, in Case V, the cup was initially positioned in a correct way (cf. angles in Table 1). However, from the extensive backside abrasive damage pattern on the UHMWPE shell, we could deduce that the ceramic liner worked for a non-negligible period of time after having been rotated by about 45° into the metal shell (cf. Fig. 5 and the thickness reduction by wear in Fig. 4(e)), thus dramatically increasing the risk of subluxation and head impingement. It should be indeed assumed that after liner rotation had occurred did the rim chipping presumably happened.

In Cases I and VI, we additionally observed a completely different pattern of fracture that can be considered to be peculiar to the sandwich-type liner. This is a circumferential crack path spanning over the entire cup, which in turn resulted in splitting of the ceramic liner into two broken hemispheres (cf. Fig. 3(a) and (f)). In Case VI, this fracture pattern was additive to rim chipping. The origin of such different crack path has not yet been discussed in the published literature. We newly suggest here that it arose from localized loading (in bending) of the convex surface of the ceramic cup after its rotation into the metal shell. The effects on fracture paths of this kind of localized loading applied on the pole of a curved brittle system with unsupported margins has been studied in detail by Rudas et al. (2005) by means of a boundary element analysis. This analysis indeed predicted (and experimentally validated) the formation of cracks, which nucleated at the pole of the cup and extended toward the dome base. Fig. 7 shows a series of drafts that attempts to comprehensively describe the sequence of degradative events that led to the observed fracture patterns. Fig. 7(a) shows a hip joint correctly implanted, in which the body weight selectively induces creep deformation in a limited interval of radial angles in the UHMWPE shell (Fig. 7(b)). Under the effect of an increased tangential force due to the local deformation of the polyethylene shell, dislodgment eventually occurred

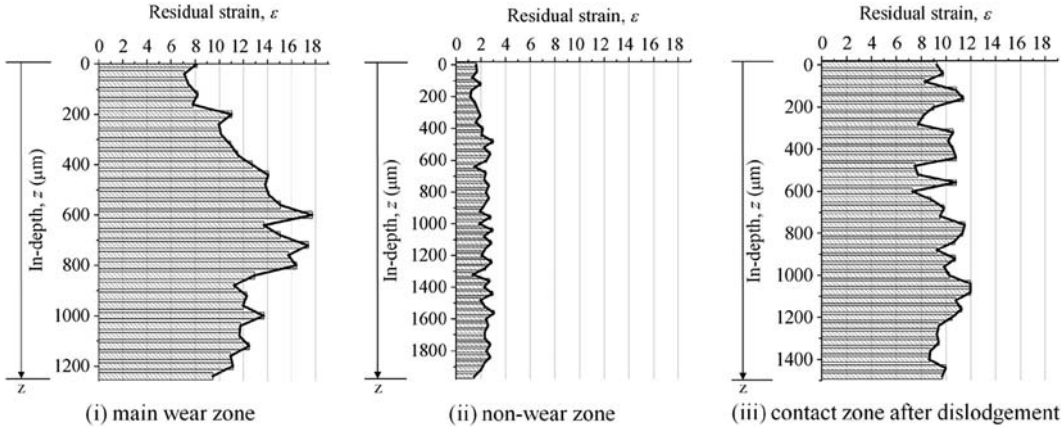

Fig. 6 – Profile of residual strain as detected along the sub-surface of the UHMWPE layer of Case VI in the main wear zone, the non-wear zone, and in the contact zone after dislodgment (labeled zone (1), (2), and (3), respectively, in Fig. 2(a)). Note that the zero point of the in-depth abscissa correspond to the side of the UHMWPE layer in contact with the ceramic liner, as shown in Fig. 2(b).

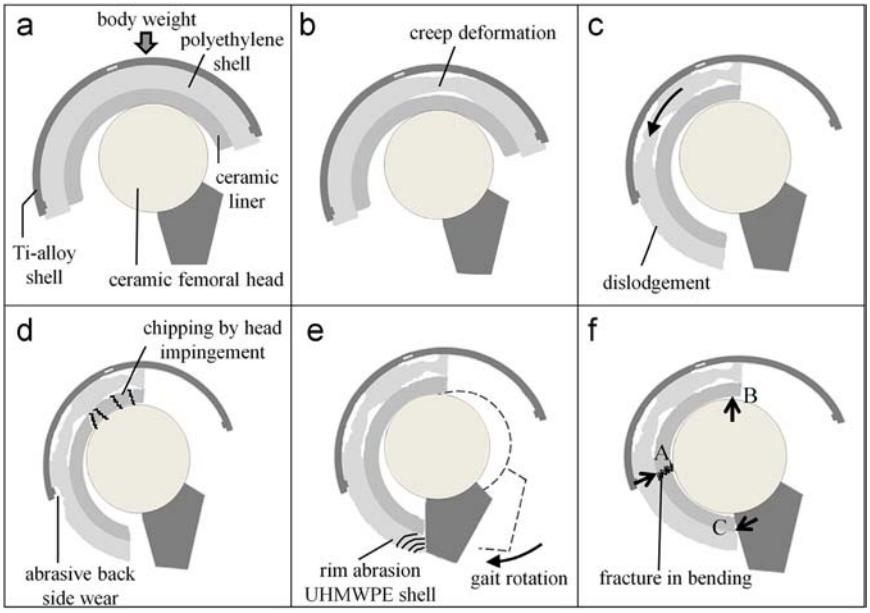

Fig. 7 – Drafts describing the sequence of degradative events that led to the observed liner fracture patterns: (a) sandwich-type hip joint correctly implanted; (b) creep deformation in a limited interval of radial angles of the UHMWPE shell due to body weight; (c) occurrence of dislodgment upon rotation of UHMWPE shell/ceramic liner inside the metal shell; (d) impingement of femoral head on the upper rim of the ceramic liner (i.e., in a state of subluxation) producing chipping of the ceramic liner; (e) impingement of the stem neck on the lower rim of the (rotated) UHMWPE shell, which in turn produced severe abrasions to the shell rim and (f) polar loading (at location A) producing bending of the curved cup component constrained by the supporting points B and C.

(Fig. 7(c)), and such an incorrect implant configuration exacerbated impingements of both femoral head on the upper rim of the ceramic liner (i.e., in a state of subluxation) and stem neck on the lower rim of the UHMWPE shell (cf. Fig. 7(d) and (e)). In addition, Fig. 7(f) schematically shows the state of localized loading on the (rotated) pole of the ceramic cup (integer to the UHMWPE shell). The loading configuration indeed foresees polar loading (at location A in Fig. 7(f)) with bending of the curved cup component upon loading reactions at the supporting points B and C in Fig. 7(f), which corresponded to the rim impingement locations of the femoral head and of the stem neck, respectively. Such loading configuration ultimately led to a single circumferential crack starting from the pole of the ceramic liner and propagating toward the cup base. Experimental evidence supporting the occurrence of such fracture mechanism was searched for on the circumferential fracture surface of the ceramic liner. As shown in Fig. 8, the fracture origin could be found in correspondence of the external surface of the ceramic liner nearby the location where polar pressure was exerted by the metallic shell (location A in Fig. 7(f)).

The complex sequence of mechanisms shown in Fig. 7 can rationally explain the phenomenological observation made on all the analyzed retrievals, with the exception of Case IV. As a matter of fact, the occurrence of multiple crack paths, the observation of no dislodgment in the radiographic preoperative exam, and the lack of any abrasive damage in the UHMWPE shell clearly reveal the occurrence of a different failure mechanism. The ceramic liner was indeed backed by the thinnest among the UHMWPE shells employed by the maker and the fracture pattern suggests a compressive

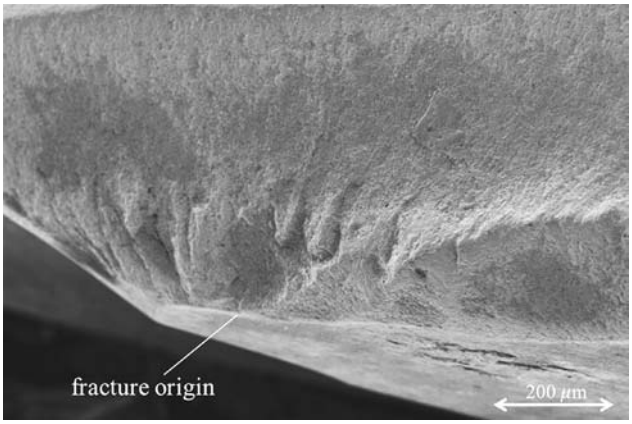

Fig. 8 – Scanning electron micrograph of the fracture origin found on the external side (convex surface) of the fractured surface of the circumferentially broken ceramic liner referred to as Case VI.

fracture event (Espinosa et al., 1998; Zavattieri and Espinosa, 2001), presumably amplified by shocks of the femoral head against the ceramic cup. Recently, Uribe et al. (2011) have presented a focused modeling study of shock-induced damages in ceramic hip prostheses. In this study, the shock-induced stress was determined numerically using finite element analysis and demonstrated that even a minor microseparation effect in an all-ceramic hip implant could cause a severe shock on the bearing surface when the heels touch the ground. Such shock can be as high as nine times the body weight. Owing to the presence of crack initiation sites on

the bearing surface (i.e., as a consequence of wear scars), one could conclude that the thickness of the ceramic liner could have resulted to be too thin to guarantee structural integrity under gait conditions in the presence of microseparation.

4. Conclusion

In conclusion, a series of six (failed) sandwich implants with *in vivo* lifetimes ranging between 2 and 9 yr (average followup of 6 yr 9 months) was studied in order to classify their mechanisms of failure and the related causes. Among the investigated implants, four implants showed fracture of the ceramic liner. Three different patterns of liner fracture could be located: (i) chipping into several pieces of the rim of the ceramic liner due to subluxation accompanied by impingement and shock of the femoral head against the liner (two cases); (ii) fracture of the liner into two hemispheres by a single circumferential crack path spanning over the entire cup (two cases, of which one also included the pattern in (i)); and (iii) fragmentation fracture of the ceramic liner into a large number of small pieces (one case). In the case of pattern (iii) (i.e., in only one case), dislodgement of the UHMWPE shell/ceramic liner was not observed in pre-operative radiographic analyses. An analysis of the failure events showed that, with the exception of the fracture pattern (iii), all the other ceramic fracture cases were a consequence of dislodgment or of implantation errors. In particular, creep of the polyethylene shell was found to be the triggering phenomenon for dislodgment and, thus, the origin of the overall sequence of failure events. We conclude that failure cases of sandwich-type implants should be classified as design failures rather than ceramic-on-ceramic fractures since no material could stand in its bearing functions when loaded in the incorrect geometry that arose from such a malfunctioning implant mechanics.

Appendix A. Supporting information

Supplementary data associated with this article can be found in the online version at http://dx.doi.org/10.1016/j.jmbbm.2013.01.022.

REFERENCES

Amino, H., 2002. Ceramic on ceramic total hip arthroplasty in Japan. Pharma Medica 20, 19–25 (in Japanese).

Bewill, SL., et al., 2005. Finite element simulation of early creep and wear in total hip arthroplasty. Journal of Biomechanics 38, 2365–2374.

Cameron, H.U., 1991. Ceramic head implantation failures. Journal of Arthroplasty 6, 185–188.

Coventry, M.B., 1985. Late dislocations in patients with Charnley total hip arthroplasty. Journal of Bone and Joint Surgery (American) 67, 832–841.

Dalla Pria, P., et al., 2010. Breakage and noises in ceramic on ceramic couplings. European Journal of Orthopaedic Traumatology 1, 53–59.

Espinosa, H.D., et al., 1998. A finite deformation continuum/discrete model for the description of fragmentation and damage in brittle materials. Journal of the Mechanics and Physics of Solids 46, 1909–1942.

Glyn-Jones, S., 2008. The creep and wear of highly cross-linked polyethylene. Journal of Bone and Joint Surgery (British) 90B, 556–561.

Ha, Y.C., et al., 2006. Ceramic liner fracture after cementless alumina-on-alumina total hip arthroplasty. Clinical Orthopaedics and Related Research 458, 106–110.

Hamadouche, M., et al., 2002. Alumina-on-alumina total hip arthroplasty: a minimum 18.5-year follow-up study. Journal of Bone and Joint Surgery: American 84, 69–77.

Hannouche, D., et al., 2003. Fractures of ceramic bearings: history and present status. Clinical Othopaedics 417, 19–26.

Hasegawa, M., et al., 2006. Cobalt–chromium head wear following revision hip arthroplasty performed after ceramic fracture —a case report. Acta Orthopaedica 77, 833–835.

Hasegawa, M., et al., 2003. Ceramic acetabular liner fracture in total hip arthroplasty with a ceramic sandwich cup. Journal of Arthroplasty 18, 658–661.

Hiss, R., et al., 1999. Hobeika S, Lynn C, Strobl G. Network stretching, slip processes, and fragmentation of crystallites during uniaxial drawing of polyethylene and related copolymers. A comparative study. Macromolecules 32, 4390–4403.

Huo, M.H., et al., 1996. Total hip replacements using the ceramic Mittelmeier prosthesis. Clinical Orthopaedics 332, 143–150.

Kaku, N., et al., 2001. Qualitative analysis of polyethylene wear in a bipolar femoral prosthesis: a case report. Journal of Orthopaedics Surgery 9, 71–76.

Kircher, J., et al., 2009. Extremely high fracture rate of a modular acetabular component with a sandwich polyethylene ceramic insertion for THA: a preliminary report. Archives of Orthopaedic and Trauma Surgery 129, 1145–1150.

Kitajima, S., Hotokebuchi, T., 2003. Ceramic on ceramic total hip arthroplasty. Journal of Joint Surgery 22, 85–89 (in Japanese).

Krikler, S.J., 1997. Fracture of a ceramic femoral head after a revision operation. A case report. Journal of Bone and Joint Surgery: American 79A, 118–121.

Kumakura, T., et al., 2009. In-depth oxidation and strain profiles in UHMWPE acetabular cups non-destructively studied by confocal Raman microprobe spectroscopy. Journal of Biomaterials Science: Polymer Edition 20, 1809–1822.

Kyomoto, M., et al., 2007. Strain in UHMWPE for orthopaedic use studied by Raman microprobe spectroscopy. Journal of Biomaterials Science: Polymer Edition 18, 165–178.

Lewinnek, G.E., et al., 1978. Dislocations after total hip-replacement arthroplasties. Journal of Bone and Joint Surgery: American 60, 217–220.

Maccauro, G., Piconi, C., 2000. Ceramic femoral head fracture in total hip replacement. International Orthopaedics 24, 239.

McCollum, D.E., Gray, W.J., 1990. Dislocation after total hip arthroplasty: causes and prevention. Clinical Orthopaedics and Related Research 261, 159–170.

McLean, C.R., et al., 2002. Delayed fracture of the ceramic femoral head after trauma. Journal of Arthroplasty 17, 503–504.

Messieh, M., et al., 1994. Wear debris from bipolar femoral neck-cup impingement: a cause of femoral stem loosening. Journal of Arthroplasty 9, 89–93.

Oonishi, H., 1992. New design feature of high-quality alumina-alumina ceramic combination in total hip replacement. Bioceramics 5, 403–408.

Park, Y.S., et al., 2006. Ceramic failure after total hip arthroplasty with an alumina-on-alumina bearing. Journal of Bone and Joint Surgery: American 88, 780–787.

Peiro, A., 1991. Fracture of the ceramic head in total hip arthroplasty: report of two cases. Journal of Arthroplasty 6, 371–374.

Pezzotti, G., et al., 2011. Non-destructively differentiating the roles of creep, wear and oxidation in long-term in vivo

exposed polyethylene cups. Journal of Biomaterials Science: Polymer Edition 22, 2165–2184.
Piconi, C., et al., 1999. Analysis of a failed alumina THR ball head. Biomaterials 20, 1637–1646.
Pulliam, I.T., Trousdale, R.T., 1997. Fracture of a ceramic femoral head after a revision operation. A case report. Journal of Bone and Joint Surgery: American 79, 118–121.
Rudas, M., et al., 2005. Failure of curved brittle layer systems from radial cracking in concentrated surface loading. Journal of Materials Research 20, 2812–2819.
Sariali, E., et al., 2009. Undetected fracture of an alumina ceramic on ceramic hip prosthesis. Journal of Arthroplasty 25 (4), 658.e1–658.e5.
Sedel, L., 2000. Evolution of alumina-on-alumina implants: a review. Clinical Orthopaedics and Related Research 379, 48–54.
Suzuki, K., 2003. Fracture of a ceramic acetabular insert after ceramic-on-ceramic THA—a case report. Acta Orthopaedica Scandinavica 74, 101–103.
Tashiro, K., et al., 1988. Morphological effect on the Raman frequency shift induced by tensile stress applied to crystalline polyoxymethylene and polyethylene: spectroscopic support for the idea of an inhomogeneous stress distribution in polymer material. Polymer 29, 1768–1783.
Tateiwa, T., et al., 2008. Ceramic total hip arthroplasty in the United States: safety and risk issues revisited. American Journal of Orthopedics 37, E26–E31.
Uribe, J., et al., 2011. Finite element modeling of shock-induced damages on ceramic hip prostheses. International Scholarly Research Network, Materials Science Article ID 121486, 1–14.
Widmer, K.H., Zurfluh, B., 2004. Compliant positioning of total hip components for optimal range of motion. Journal of Orthopaedic Research 22, 815–821.
Willmann, G., 2001. Retrieved ceramic wear couple: unexpected findings. In: Toni, A., Willmann, G. (Eds.), Bioceramics in Joint Arthroplasty: Proceedings of the 6th BIOLOX® Symposium. Georg Thieme Verlag, Stuttgart, Germany, pp. 63–65.
Wong, W.F., Young, R.J., 1994. Molecular deformation processes in gel-spun polyethylene fibres using Raman spectroscopy. Journal of Materials Science 29, 510–519.
Woo, R.Y., Morrey, B.F., 1982. Dislocations after total hip arthroplasty. Journal of Bone and Joint Surgery: American 64, 1295–1306.
Yamaguchi, M., et al., 2000. The spatial location of impingement in total hip arthroplasty. Journal of Arthroplasty 15, 305–313.
Yamamoto, K., et al., 2004. Failure of ceramic THR with liner dislocation—a case report. Acta Orthopaedica Scandinavica 75, 500–502.
Zavattieri, P.D., Espinosa, H.D., 2001. Grain level analysis of crack initiation and propagation in brittle materials. Acta Materialia 49, 4291–4311.